Assessment of mechanical properties of bone trabeculae as an inverse problem of heterogeneous material modeling

K Janc, J Tarasiuk, P Lipinski, A.-S Bonnet, S Wronski

ARCHIVES OF MECHANICS
Arch. Mech. **72** (5), 385–414, 2020, DOI: 10.24423/aom.3469

Assessment of mechanical properties of bone trabeculae as an inverse problem of heterogeneous material modeling

K. JANC[1)], J. TARASIUK[1)], P. LIPINSKI[2)], A.-S. BONNET[2)], S. WRONSKI[1)]

[1)] *Faculty of Physics and Applied Computer Science (WFiIS), AGH – University of Science and Technology, 30 Mickiewicza Ave., 30-059 Kraków, Poland, e-mails: krzysztof.janc@gmail.com, tarasiuk@agh.edu.pl, wronski.sebastian@gmail.com*

[2)] *LEM3, Université de Lorraine, Ecole Nationale d'Ingénieurs de Metz, 1 Route d'Ars Laquenexy, BP 65820, 57 078 Metz Cedex 03, France, e-mails: pawel.lipinski@univ-lorraine.fr, anne-sophie.bonnet@univ-lorraine.fr*

In this study, the trabecular bone was treated as a composite material that consists of a bone matrix weakened by ellipsoidal pores. Under the hypothesis that all information concerning the local properties and the microarchitecture are "encrypted" in the apparent properties of a given volume element (VE) of the bone, a method of retrieving these data was proposed. Software based on a genetic algorithm, combined with the incremental scale transition method was developed to this end. To test the approach, μCT measurements of four bone samples were performed providing their real micro-architecture. Tensors of apparent properties of the samples were next computed by numerical (finite element) homogenization method for a large range of the elastic properties of trabeculae. They were considered as the fitness function for the proposed algorithm. Very good agreement was found between the obtained and target values of the apparent elastic properties of the samples and volume fraction of pores. The approach is fast and accurate enough in comparison to the finite element homogenization. As an auxiliary result it was shown that the anisotropy of apparent elastic properties is mainly related to the microarchitecture of the bone, not to the intrinsic properties of trabeculae.

Key words: bone mechanical properties, inverse problem, computer modelling, incremental scheme.

1. Introduction

Mammals' bones are constituted of two types of tissues: cortical (or compact) bone and trabecular (or spongy) one. Cortical tissue is a dense matter situated on the periphery of bones whereas cancellous tissue is a highly porous material forming their core. The microstructure of cancellous bone consists of a network of trabeculae. The typical size of an individual trabecula of the human femur is around $100 \times 500 \times 1000$ μm^3. So, the use of classical mechanical tests to

assess its elastic properties is ill-adapted. Consequently, ultrasonic measurements have been frequently applied [1, 2] to estimate the bone elastic constants. Also, the nanoindentation technique was successfully used [3, 4] to identify the Young's modulus of the trabeculae. More recently, a new device enabling the measurement of the elastic modulus of an individual strut of spongy bone through the 3-point bending test has been proposed [5].

On the other hand, models have been proposed to estimate the elastic modulus of a porous solid in terms of its density [6]. Although, density of trabecular bone has a significant influence on its apparent properties, on its own it cannot fully reflect bone's mechanical behaviour. To characterize more precisely this behaviour, information about the trabecular bone architecture, characterized by the thickness, number and distance between individual trabeculae and their 3D network have to be provided.

Therefore, several authors [7–10] used high-resolution images of trabecular bone samples obtained from μCT scans to predict the elastic moduli of bone through finite element modelling. Other analyses [11, 12] were based on an idealized periodic geometry of trabecular bone, composed of networks of beams and/or plates, instead of its actual geometry. Voronoi techniques [13] were also used to generate a non-periodic mesh imitating the trabecular bone.

Trabecular bone can also be regarded as a very competing composite. To describe the effective properties of composite materials, more or less complicated models were developed. Most of these methods were elaborated for modelling two-phase composites rather than bone. For instance, Voigt and Reuss estimates [14, 15] can be cited as coarse approximations of the elastic properties of heterogeneous materials. Voigt assumed that each phase of composite material undergoes the same strain (homogeneous strain field). In the case of a two-phase material with properties defined by tensors of elastic moduli $\boldsymbol{c}^1$ and $\boldsymbol{c}^2$, the Voigt approximation of effective elastic moduli of composite $\boldsymbol{C}^V$ is defined as the volume weighted average of the phase properties and becomes:

$$\boldsymbol{C}^V = f_1\boldsymbol{c}^1 + f_2\boldsymbol{c}^2 = \langle \boldsymbol{c}^I \rangle, \qquad I = 1, 2 \tag{1.1}$$

where $f_1 = V_1/V$ and $f_2 = V_2/V = 1 - f_1$ are the volume fractions of both phases of volumes V_1 and V_2, respectively and $V = V_1 + V_2$ represents the total volume of the composite.

On the other hand, Reuss assumed the condition of uniform stress in all phases enabling evaluation of the effective elastic moduli tensor $\boldsymbol{C}^R$. For a two-phase composite it leads to:

$$\boldsymbol{C}^R = [f_1(\boldsymbol{c}^1)^{-1} + f_2(\boldsymbol{c}^2)^{-1}]^{-1}. \tag{1.2}$$

Voigt and Reuss approximations take into consideration exclusively the volume fractions of the constituents and therefore furnish a very rough estimate of the

real composite behaviour. It can be shown that they provide the upper and lower bounds for the elastic moduli of a composite material. To improve the description, various models were proposed taking into account more details of the internal structure (or microarchitecture) of materials. The complexity of the microstructure is mathematically reflected by the fourth-order localisation tensors. In the case of kinematic approach, the strain localisation tensor $\boldsymbol{A}(\boldsymbol{r})$ is considered. Following HILL [16], it is defined by the relation below:

$$\boldsymbol{\varepsilon}(\boldsymbol{r}) = \boldsymbol{A}(\boldsymbol{r}) : \boldsymbol{E}. \tag{1.3}$$

It allows the determination of the effective elastic properties $\boldsymbol{C}^{\text{eff}}$ of the VE:

$$\boldsymbol{C}^{\text{eff}} = \frac{1}{\boldsymbol{V}} \int\limits_{V} \boldsymbol{c}(\boldsymbol{r}) : \boldsymbol{A}(\boldsymbol{r})\, dV. \tag{1.4}$$

To establish a general approach allowing the determination of this concentration tensor, we remind the formal solution describing the deformation of the representative volume of an inhomogeneous material under homogeneous boundary conditions of Dirichlet type. This solution is called kinematical integral equation and has been proposed in elasticity initially by Elmer and generalised by DEDERICHS and ZELLER [17].

To obtain this integral equation, the Green tensor is used, established for the case of the infinite body with the homogeneous reference properties $\boldsymbol{C}^{\boldsymbol{r}}$. All details of such an approach are given for example in the works [17–19]. The final solution takes the form of integral equations expressing the displacement and strain fields of heterogeneous material volume.

$$\vec{\boldsymbol{u}}(\boldsymbol{r}) = \vec{\boldsymbol{U}}^{\boldsymbol{r}}(\boldsymbol{r}) + \int\limits_{\boldsymbol{V}} \frac{\partial \boldsymbol{G}(r - \boldsymbol{r}')}{\partial \boldsymbol{r}} : \delta \boldsymbol{c}(\boldsymbol{r}') \boldsymbol{\varepsilon}(\boldsymbol{r}')\, dV', \tag{1.5}$$

$$\begin{aligned} \boldsymbol{\varepsilon}(\boldsymbol{r}) &= \boldsymbol{E}^{\boldsymbol{r}} + \int\limits_{\boldsymbol{V}} \frac{\partial^2 \boldsymbol{G}(\boldsymbol{r} - \boldsymbol{r}')}{\partial \boldsymbol{r} \partial \boldsymbol{r}} : \delta \boldsymbol{c}(\boldsymbol{r}') : \boldsymbol{\varepsilon}(\boldsymbol{r}')\, dV' \\ &= \boldsymbol{E}^{\boldsymbol{r}} + \int\limits_{\boldsymbol{V}} \boldsymbol{\Gamma}(\boldsymbol{r} - \boldsymbol{r}') : \delta \boldsymbol{c}(\boldsymbol{r}') : \boldsymbol{\varepsilon}(\boldsymbol{r}')\, dV'. \end{aligned} \tag{1.6}$$

The following new quantities have appeared in these expressions:

$\vec{\boldsymbol{U}}^{\boldsymbol{r}}(\boldsymbol{r})$ – displacement field of the reference medium,

$\boldsymbol{G}(\boldsymbol{r} - \boldsymbol{r}')$ – the Green tensor of the elasticity problem describing the displacement at point $\boldsymbol{r}$ due to the unit force applied at point $\boldsymbol{r}'$.

$\boldsymbol{\Gamma}(\boldsymbol{r} - \boldsymbol{r}') = \frac{\partial^2 \boldsymbol{G}(\boldsymbol{r} - \boldsymbol{r}')}{\partial \boldsymbol{r} \partial \boldsymbol{r}}$ – modified Green tensor,

$\boldsymbol{E}^{\boldsymbol{r}}$ – homogeneous strain field of the reference medium which is generally different from the imposed strain $\boldsymbol{E}$,

$\delta \boldsymbol{c}(\boldsymbol{r}) = \boldsymbol{c}(\boldsymbol{r}) - \boldsymbol{C^r}$ – the deviation part of local properties from the properties of reference medium $\boldsymbol{C^r}$.

Expressions (1.5) and (1.6) constitute the formal solution of the problem and allow us to deduce a form of the concentration tensor $\boldsymbol{A}(r)$.

In most cases, models deduced from the integral Eq. (1.6) are based on the solution of the ellipsoidal inclusion problem originated by Eshelby.

Suppose that the VE is composed of N reinforcements enumerated from 1 to N and a surrounding matrix which is considered as a constituent number 0. We admit that the geometry of reinforcements can be approached by ellipsoidal inclusions. As a consequence, the composite is made up with $(N+1)$ constituents. The volume of a given inclusion I, or family of the same type of inclusions, is noted V^I. If the volume of VE is supposed to be V, the volume fraction of this inclusion is equal to:

$$f^I = \frac{V^I}{V}.$$

Let us suppose that the elastic properties of each constituent are homogeneous. In agreement with the proposed labelling of constituents, the tensor of the matrix elastic properties is noted $\boldsymbol{c}^0$ and this of inclusion $\boldsymbol{c}^I$. By consequence, the field of the elastic properties of the composite material can be expressed as below:

$$\boldsymbol{c}(r) = \boldsymbol{c}^0 \theta^0(\boldsymbol{r}) + \sum_{I=1}^{I} \boldsymbol{c}^I \theta^I(\boldsymbol{r})$$

where $\theta^I(\boldsymbol{r})$ is a characteristic function verifying the conditions:

$$\theta^I(\boldsymbol{r}) = \begin{cases} 1 & \forall \boldsymbol{r} \in V^I, \\ 0 & \text{otherwise.} \end{cases}$$

The deviation part of the elastic properties field with respect to the reference medium can now be expressed as:

$$\delta \boldsymbol{c}(r) = (\boldsymbol{c}^0 - \boldsymbol{C}^r)\theta^0(\boldsymbol{r}) + \sum_{I=1}^{I} (\boldsymbol{c}^I - \boldsymbol{C}^r)\theta^I(\boldsymbol{r}) = \Delta \boldsymbol{c}^0 \theta^0(\boldsymbol{r}) + \sum_{I=1}^{I} \Delta \boldsymbol{c}^I \theta^I(\boldsymbol{r}).$$

Substituting this result into integral Eq. (1.6) and remembering that $\theta^I(\boldsymbol{r}) = 0$ outside the reinforcement I, one gets:

$$\boldsymbol{\varepsilon}(\boldsymbol{r}) = \boldsymbol{E^r} + \int_{\boldsymbol{V}^0} \boldsymbol{\Gamma}(\boldsymbol{r} - \boldsymbol{r}') : \Delta \boldsymbol{c}^0 : \boldsymbol{\varepsilon}(\boldsymbol{r}')\, dV' + \sum_{I=1}^{N} \int_{\boldsymbol{V}^I} \boldsymbol{\Gamma}(\boldsymbol{r} - \boldsymbol{r}') : \Delta \boldsymbol{c}^I : \boldsymbol{\varepsilon}(\boldsymbol{r}')\, dV'. \tag{1.7}$$

The above equation remains very difficult to treat because of the potential complexity of the strain field $\boldsymbol{\varepsilon}(\boldsymbol{r})$. Limiting our considerations to the case of mean field approximation, the real strain field can be represented by a piecewise function below:

$$\boldsymbol{\varepsilon}(\boldsymbol{r}) = \boldsymbol{\varepsilon}^0\theta^0(\boldsymbol{r}) + \sum_{I=1}^{I} \boldsymbol{\varepsilon}^I\theta^I(\boldsymbol{r}).$$

This assumption simplifies definitely the kinematic integral equation leading to

$$\boldsymbol{\varepsilon}(\boldsymbol{r}) = \boldsymbol{E}^{\boldsymbol{r}} + \int\limits_{\boldsymbol{V}^0} \boldsymbol{\Gamma}(\boldsymbol{r}-\boldsymbol{r}')\,dV' : \Delta\boldsymbol{c}^0 : \boldsymbol{\varepsilon}^0 + \sum_{I=1}^{N} \int\limits_{\boldsymbol{V}^I} \boldsymbol{\Gamma}(\boldsymbol{r}-\boldsymbol{r}')\,dV' : \Delta\boldsymbol{c}^I : \boldsymbol{\varepsilon}^I.$$

The above equation describes the strain field of the composite. To establish the strain localisation tensors the mean strain has to be calculated for each constituent J in turn using the obvious relation:

$$\boldsymbol{\varepsilon}^J = \frac{1}{V^J} \int\limits_{\boldsymbol{V}^J} \boldsymbol{\varepsilon}(\boldsymbol{r})\,dV.$$

This yields the following result:

$$\begin{aligned}\boldsymbol{\varepsilon}^J = \boldsymbol{E}^{\boldsymbol{r}} &+ \frac{1}{V^J} \int\limits_{V^J}\int\limits_{V^0} \boldsymbol{\Gamma}(\boldsymbol{r}-\boldsymbol{r}')\,dV'\,dV : \Delta\boldsymbol{c}^0 : \boldsymbol{\varepsilon}^0 \\ &+ \sum_{I=1}^{N} \frac{1}{V^J} \int\limits_{V^J}\int\limits_{V^I} \boldsymbol{\Gamma}(\boldsymbol{r}-\boldsymbol{r}')\,dV'\,dV : \Delta\boldsymbol{c}^I : \boldsymbol{\varepsilon}^I.\end{aligned}$$

The double integrals in this equation define the so-called interaction tensors $\boldsymbol{T}^{JI}$ verifying the evident relation below:

$$V^J\boldsymbol{T}^{JI} = \int\limits_{V^J}\int\limits_{V^I} \boldsymbol{\Gamma}(\boldsymbol{r}-\boldsymbol{r}')\,dV'\,dV = \int\limits_{V^I}\int\limits_{V^J} \boldsymbol{\Gamma}(\boldsymbol{r}-\boldsymbol{r}')\,dV'\,dV = V^I\boldsymbol{T}^{IJ}.$$

The interaction tensors of ellipsoidal inclusions have been studied among others by FASSI-FEHRI *et al.* [20]. A numerical computation of these tensors has been developed by LIPINSKI [21]. Using the above notations the integral equation can be simply rewritten as:

$$\boldsymbol{\varepsilon}^J = \boldsymbol{E}^{\boldsymbol{r}} + \boldsymbol{T}^{J0} : \Delta\boldsymbol{c}^0 : \boldsymbol{\varepsilon}^0 + \sum_{I=1}^{N} \boldsymbol{T}^{JI}\Delta\boldsymbol{c}^I : \boldsymbol{\varepsilon}^I. \tag{1.8}$$

Two points make the treatment of this equation difficult. First point concerns the computation of the tensors $\boldsymbol{T}^{J0}$. Because of its very convoluted shape, the matrix cannot be approximated by an ellipsoidal inclusion and the tensors cannot be computed using the approach proposed in [20]. The choice of the matrix as a reference medium $\boldsymbol{C}^r = \boldsymbol{c}^0$ enables circumventing this difficulty. Indeed, in such a case

$$\Delta \boldsymbol{c}^0 = \boldsymbol{c}^0 - \boldsymbol{C}^r = 0$$

and the integral Eq. (1.8) can be rewritten as follows:

$$\boldsymbol{\varepsilon}^J = \boldsymbol{E}^0 + \sum_{I=1}^{N} \boldsymbol{T}^{JI} : \Delta \boldsymbol{c}^I : \boldsymbol{\varepsilon}^I. \tag{1.9}$$

where $\boldsymbol{E}^0$ represents the mean strain field of the matrix. The Mori–Tanaka one-site model is based on such a hypothesis. In fact, when the interactions among reinforcements can be neglected ($\boldsymbol{T}^{JI} \cong 0$) relation (1.9) provides the Mori–Tanaka model:

$$\boldsymbol{\varepsilon}^I = \boldsymbol{E}^0 + \boldsymbol{T}^{II} : \Delta \boldsymbol{c}^I : \boldsymbol{\varepsilon}^I,$$

or

$$\boldsymbol{\varepsilon}^I = (\boldsymbol{I} - \boldsymbol{T}^{II} : \Delta \boldsymbol{c}^I)^{-1} : \boldsymbol{E}^0$$

where $\boldsymbol{I}$ is a fourth rank unit tensor. However, it should be strongly emphasised that expression (1.9) is more general than Mori–Tanaka [22] scheme since it takes into account, through $\boldsymbol{T}^{IJ}$ tensors, the mutual interactions among the constituents.

Secondly, relation (1.8) or (1.9) constitutes an implicit solution of the problem since the unknown strain $\boldsymbol{\varepsilon}^J$ is given in function of itself and remaining tensors $\boldsymbol{\varepsilon}^I$. An iterative approach is necessary to bypass this point. To facilitate the implementation of the iterative treatment of expression (1.9) it can be transformed to:

$$\boldsymbol{\varepsilon}^J = \boldsymbol{E}^0 + \sum_{I=1,\, I\neq J}^{N} \boldsymbol{T}^{JI} : \Delta \boldsymbol{c}^I : \boldsymbol{\varepsilon}^I + \boldsymbol{T}^{JJ} : \Delta \boldsymbol{c}^J : \boldsymbol{\varepsilon}^J$$

or equivalently:

$$\boldsymbol{\varepsilon}^J = (\boldsymbol{I} - \boldsymbol{T}^{JJ} : \Delta \boldsymbol{c}^J)^{-1} : \left(\boldsymbol{E}^0 + \sum_{I=1,\, I\neq J}^{N} \boldsymbol{T}^{JI} : \Delta \boldsymbol{c}^I : \boldsymbol{\varepsilon}^I \right). \tag{1.10}$$

The evaluation of the localisation tensor can now be undertaken. Let us suppose the existence of an alternative strain localisation tensor $\boldsymbol{a}^{\mathbf{I}}$, computed with respect to the reference medium, such that:

$$\boldsymbol{\varepsilon}^{\boldsymbol{I}} = \boldsymbol{a}^{\boldsymbol{I}} : \boldsymbol{E}^0. \tag{1.11}$$

Admit also the initial or zero approximation of this tensor to be[1]:

$$\boldsymbol{a}^{\boldsymbol{I}}_{(0)} = \boldsymbol{I}.$$

This assumption is equivalent to Taylor's approximation $\boldsymbol{\varepsilon}^{\boldsymbol{I}}_{(0)} \approx \boldsymbol{E}^0$. Introducing this estimate into the second member of (1.10), the first order approximation of strain field $\boldsymbol{\varepsilon}^J_{(1)}$ is easily deduced:

$$\boldsymbol{\varepsilon}^J_{(1)} = (\boldsymbol{I} - \boldsymbol{T}^{JJ} : \Delta\boldsymbol{c}^J)^{-1} : \left(\boldsymbol{I} + \sum_{I=1}^{N} \boldsymbol{T}^{JI} : \Delta\boldsymbol{c}^I : \boldsymbol{a}^{\boldsymbol{I}}_{(0)}\right) : \boldsymbol{E}^0.$$

By comparison with (1.11) we also get:

$$\boldsymbol{a}^I_{(1)} = (\boldsymbol{I} - \boldsymbol{T}^{JJ} : \Delta\boldsymbol{c}^J)^{-1} : \left(\boldsymbol{I} + \sum_{J=1}^{N} \boldsymbol{T}^{IJ} : \Delta\boldsymbol{c}^J : \boldsymbol{a}^{\boldsymbol{I}}_{(0)}\right).$$

This new approximation of $\boldsymbol{\varepsilon}^I$ can be introduced to (1.10) to derive second order results.

$$\boldsymbol{\varepsilon}^J_{(2)} = (\boldsymbol{I} - \boldsymbol{T}^{JJ} : \Delta\boldsymbol{c}^J)^{-1} : \left(\boldsymbol{I} + \sum_{I=1}^{N} \boldsymbol{T}^{JI} : \Delta\boldsymbol{c}^I : \boldsymbol{a}^I_{(1)}\right) : \boldsymbol{E}^0 = \boldsymbol{a}^J_{(2)} : \boldsymbol{E}^0.$$

KRÖNER [23, 24] has proved that this iterative procedure is monotonically convergent to the exact values of $\boldsymbol{\varepsilon}^{\boldsymbol{I}}$ and $\boldsymbol{a}^{\boldsymbol{I}}$.

After n steps, the strain localisation tensor can be written as follows:

$$\boldsymbol{a}^I_{(n)} = (\boldsymbol{I} - \boldsymbol{T}^{JJ} : \Delta\boldsymbol{c}^J)^{-1} : \left(\boldsymbol{I} + \sum_{I=1}^{N} \boldsymbol{T}^{JI} : \Delta\boldsymbol{c}^I : \boldsymbol{a}^I_{(n-1)}\right). \tag{1.12}$$

After convergence, the localization tensors $\boldsymbol{A}^I$ with respect to the effective medium are calculated. Applying the volume average to relation (1.11) we get:

$$\boldsymbol{E} = \langle \boldsymbol{\varepsilon}^I \rangle = \langle \boldsymbol{a}^{\boldsymbol{I}} \rangle : \boldsymbol{E}^0$$

allowing the calculation of $\boldsymbol{E}^0$ as a function of $\boldsymbol{E}$:

$$\boldsymbol{E}^0 = \langle \boldsymbol{a}^{\boldsymbol{I}} \rangle^{-1} : \boldsymbol{E}.$$

Combining this last result with (1.11) yields the relation for the strain localisation tensor:

$$\boldsymbol{A}^I = \boldsymbol{a}^I : \langle \boldsymbol{a}^I \rangle^{-1}. \tag{1.13}$$

[1]To accelerate the convergence the Mori–Tanaka approximation of this initial localisation tensor $\boldsymbol{a}^{\boldsymbol{I}}_{(0)} = (\boldsymbol{I} - \boldsymbol{T}^{II} : \Delta\boldsymbol{c}^I)^{-1}$ can be used instead of $\boldsymbol{a}^{\boldsymbol{I}}_{(0)} = I$.

Such a generalized "Mori–Tanaka" scheme is quite well suited for modelling the mechanical properties of materials with small fractions of reinforcements. However, as it was demonstrated by Broohm *et al.* [25], in the case of composites characterized by a high contrast between the matrix and reinforcement properties, such as for instance the cancellous bone, the models of Mori-Tanaka type do not perform well. To obtain a more accurate approximation for larger volume fractions of the voids, the differential scheme, first proposed by Bruggeman [26] can be applied. In this work, an incremental version of this approach, proposed in [27], is exploited.

The paper is organized as follows. Section 2 is dedicated to the description of the method used to collect the apparent bone properties. Some additional details on the Incremental Scheme (IS) are next presented and the bases of the optimization procedure are reminded. Section 3 is devoted to the analysis and discussion of obtained results. First, the outcomes of microstructure fitting are presented. The sensitivity of the method was tested with respect to the values of elastic properties of the trabeculae and the bone porosity. Finally, the full inverse problem results are given and supplemented by some general comments.

2. Materials and methods

2.1. Collection of apparent bone properties

Four cubic samples (numbered I to IV) sized $10 \times 10 \times 10$ mm^3 were cut off from the neck of porcine femoral bones. Each sample was scanned using Nanotom 180N device (GE Sensing & Inspection Technologies phoenix| X-ray Gmbh). The machine is equipped with Nanofocus X-ray tube with maximal voltage of 180 kV. The tomograms were registered on the Hamamatsu 2300×2300 pixel detector. The numerical reconstruction of scanned objects was done with the aid of proprietary GE software DatosX ver. 2.1.0. It makes use of an algorithm [28] developed for cone beam X-ray CT. All examined specimens were scanned at 60 kV of source voltage and 310 μA. The 360° rotation of the specimen was completed in 1800 steps. The exposure time was 500 ms and a frame averaging of 5 and image skip of 1 was applied, resulting in a scanning time of 90 minutes. The reconstructed images had a voxel size of 10 μm^3. The post reconstruction data treatment was completed by VGStudio Max 2.1 and free Fiji software with BoneJ plug-in [29, 30].

The scans of the samples were binarized following Otsu method [31], i.e. the pixels of individual images were sorted into two media: bone and the rest. On the basis of these binarized scans, 3D structures were reconstructed.

For the purpose of this paper the apparent elastic properties of the bone samples were obtained by the FEM, or numerical homogenization, instead of

the experimental measurements. The advantage of such an approach is that the trabeculae properties, which constitute the input data for FEM, could directly be compared with the matrix properties issued from the optimization process. Large ranges of Young's moduli and Poisson's ratios of trabeculae were tested to validate the approach. Due to the gradient of porosity and time of calculations using FEM homogenization, smaller cubes with the edge of 5 mm were isolated numerically from each sample. The cubes were extricated in a way that the main axes of material symmetry frame were perpendicular or parallel to the walls of the resulting sample. Such 3D objects were next meshed using first order hexagonal elements.

The mean size of elements was chosen to be 25 μm. On average, the obtained meshes involve about 3 800 000 elements and 5 050 000 nodes with three degrees of freedom per node. Example of a 3D object (sample I), its mesh and the zoom on one of its corners are illustrated in Fig. 1.

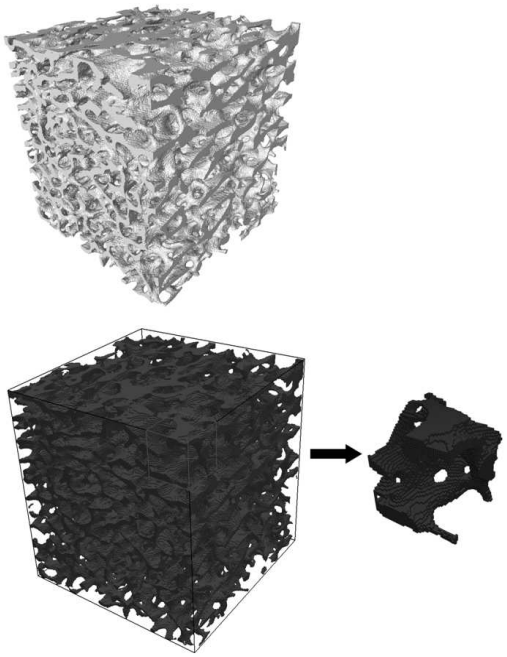

FIG. 1. Example of 3D reconstruction and mesh of the trabecular bone sample I. Top image: 3D reconstruction from μCT, bottom images: FE mesh and the zoom on its upper-right corner.

A series of simple mechanical loads (compression and shear) was simulated in order to determine the samples' apparent elastic properties ($E_1, E_2, E_3, G_{23}, G_{31}, G_{21}, \nu_{23}, \nu_{13}, \nu_{12}$). The periodicity conditions were applied on appropriate faces of

the meshes, function of the load type considered. More details about the meshing and boundary conditions used can be found in [32]. Besides, the porosity of each sample was calculated from the ratio between the volume of the finite element mesh and the apparent volume of the corresponding cubic envelopes (125 mm^3). All finite element simulations were carried out with ABAQUS Software (Dassault Systèmes), version 6.14.

2.2. Multi-site Incremental Modelling of bone sample

The incremental scheme (IS) was successfully used to model composite or heterogeneous materials with complicated microstructures [27, 34]. The method involves a progressive, or step-by-step, placing of reinforcements into the matrix followed by homogenization operation, i.e. for every step s the average properties of such an "intermediate" material are calculated. This material is considered as the matrix for the next step of the composite construction (see Fig. 2).

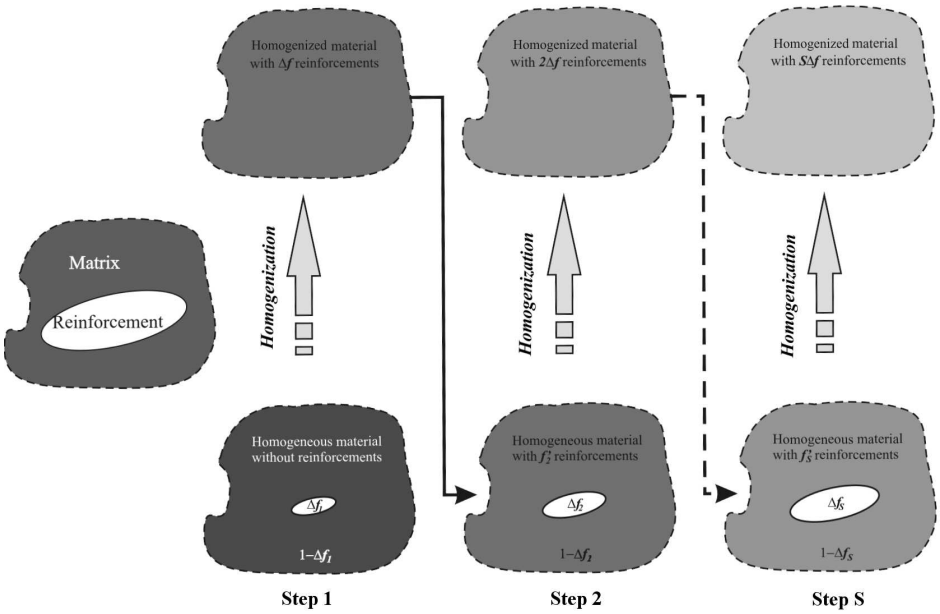

FIG. 2. Construction of a homogeneous material using the Incremental Scheme idea.

Let S be the total number of steps used to build the composite. To preserve the proportional increase of reinforcement volume fractions through the stepping procedure, the value Δf_s^{I} of the new fraction of inclusions I should be determined for each step s. This value is different from f^{I}/S and is equal to:

$$\Delta f_s^{\mathrm{I}} = r_s f^{\mathrm{I}} \tag{2.1}$$

where f^{I} is the final or desired volume fraction of inclusion I. The coefficient r_s is given by the expression:

$$r_s = 1/[S - (s-1)(1 - f^0)] \tag{2.2}$$

in which f^0 states for the matrix volume fraction. As expected, at first step, for which the reference medium is a pure matrix, this value is equal to $\Delta f_1^I = f^{\mathrm{I}}/S$. However, for the next steps $\Delta f_s^{\mathrm{I}} > f^I/S$. It is due to the fact that, to insert the new volume fraction of reinforcements, an appropriate part of the reference medium, is replaced by them. But this medium contains already the inclusions. The shadows of grey, used to represent the reference medium in Fig. 2, depict this fact. The point of increasing Δf_s^{I} is illustrated in the same figure by augmenting size of inclusions. The proof of (2.2) can be found for instance in [25] or [27].

The effective material properties obtained by the Incremental Scheme $(C^{\mathrm{IS}})_{s+1}$ after step $s+1$ are derived using the following equation:

$$(C^{\mathrm{IS}})_{s+1} = (C^{\mathrm{IS}})_s + r_s \sum_{I=1}^{N} f^I (\Delta \boldsymbol{c}^{\mathrm{I}})_s : (\boldsymbol{A}^{\mathrm{I}})_s \tag{2.3}$$

where

$$(\Delta \boldsymbol{c}^I)_s = \boldsymbol{c}^{\mathrm{I}} - (\boldsymbol{C}^{\mathrm{IS}})_s \tag{2.4}$$

and N indicates the number of reinforcement's families. The algorithm calculating the values of effective properties begins assuming that $(C^{\mathrm{IS}})_0 = c^0$. To determine the localization tensors $(A^{\mathrm{I}})_s$, expressions (1.12) and (1.13) are used at each step. More details on Mori–Tanaka method combined with IS can be found in reference [34]. A Periodic Cell (PC), formed by a matrix and weakened by a pattern of ellipsoidal voids, is considered. The size of PC is specified by three variables Δx, Δy and Δz corresponding to the length of its three edges, see Fig. 3 illustrating the concept of PC in 2D.

Information concerning the size of the PC is necessary to delimitate the position of the inclusions centre and to define the periodic repetition of PC in the Volume Element (VE). Also, the number N of desired inclusions representing reinforcement pattern must be specified. The number of interacting inclusions depends on the choice of Radius of Interaction (RI). For a given inclusion I from the PC, the interaction tensors $\boldsymbol{T}^{\mathrm{IJ}}$ are calculated for all inclusions J such that the distance d between the centres of I and J are smaller than RI. Knowing that the values of $\boldsymbol{T}^{\mathrm{IJ}}$ components decrease very rapidly with the distance between inclusions' centres (they are proportional to d^{-3}) only the first neighbours of I can be considered. The results presented in this work were obtained for $RI = \Delta x$ and $N = 4$. It corresponds to approximately 50 mutually interacting inclusions. The exact number depends on the morphology and topology of the PC.

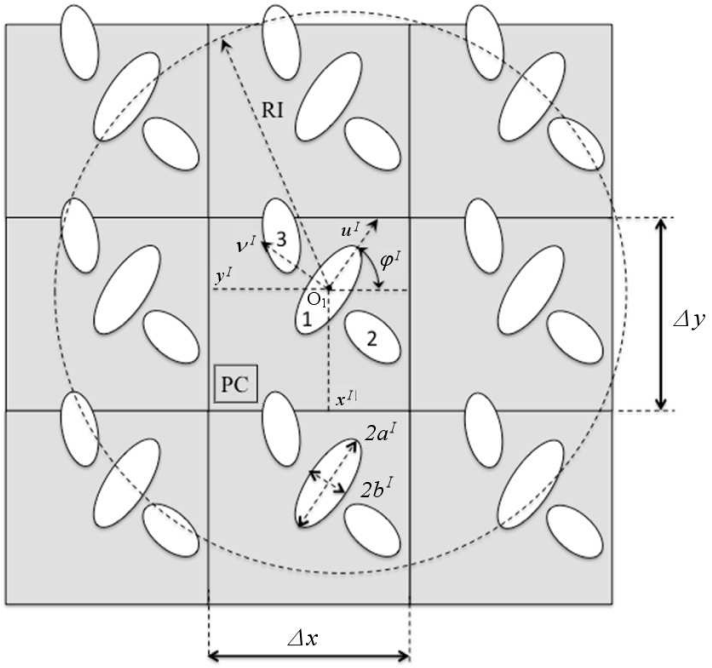

Fig. 3. Schematic (2D) representation of a Periodic Cell (PC) with 3 inclusions and their first periodically distributed neighbors.

For the description of each inclusion I, the location of its center, expressed by three coordinates x^{I}, y^{I}, z^{I} has to be specified. The position is expressed in the global coordinates system of the periodic cell. The following three parameters, a^{I}, b^{I} and c^{I}, describe the geometry of the ellipsoid and more precisely the length of its three semi-axes parallel to a local coordinate system $(O^{\mathrm{I}}; u^{\mathrm{I}}, v^{\mathrm{I}}, w^{\mathrm{I}})$ with its origin O^{I} located at the center of the ellipsoid I. Initially, these semi-axes have the unit length and are parallel to the borderlines of the PC. During the optimization process, the lengths and orientation of every inclusion evolve. Their subsequent orientations are defined by three Euler's angles φ^I, ϕ^I and θ^I. These data are sufficient to compute the volume fractions of constituents.

In the applications presented in the next paragraph, the elastic properties of the matrix are supposed to be isotropic as in the FE calculations. Therefore, for their description, only the Young's modulus E_m and Poisson's ratio ν_m are required. The volume fraction of the matrix can be determined as a complement to 1 of the sum of volume fractions of all inclusions. In the case where interactions between the inclusions are negligible (one site approach), all reinforcements with the same orientations and ratios of semi axes can be represented by only one inclusion whose volume fraction is the sum of the fractions of inclusions

being substituted. However, in this case, the volume fraction of inclusions is not necessarily compatible with the geometric volume fraction of the matrix. In such a configuration, the value of the volume fraction of inclusions is therefore added as an independent parameter. In the presented approach, the void inclusions are used to model bone porosity, so their mechanical properties are constant and defined by the zero tensor. As a result, in general case, the VE is described by $10N + 2$ parameters, where N is the number of involved ellipsoidal inclusions.

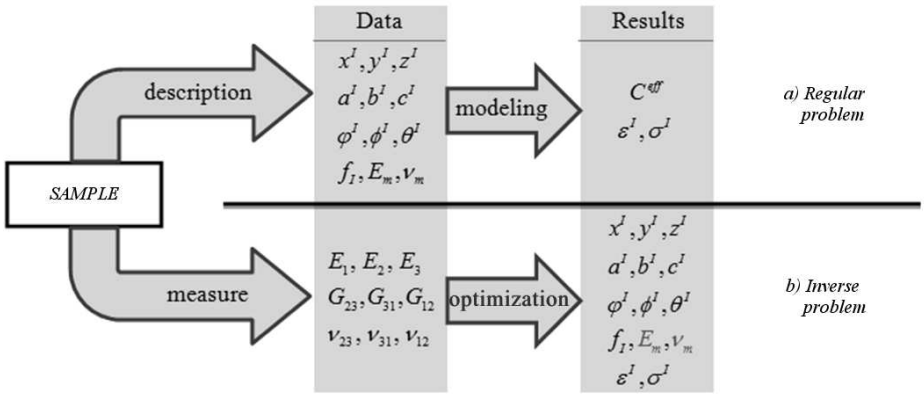

FIG. 4. The difference between regular and inverse problems in homogenization schemes.

The usual or regular situation of using homogenization methods consists in the definition of a representative volume of heterogeneous material by specifying the mechanical properties of phases, their shapes and orientations with respect to some fixed coordinate frame. The main aims of these methods are the description of global or overall properties and local mechanical fields such as stresses and strains. This situation is sketched in Fig. 4a in the case of an isotropic matrix with Young's modulus E_m and Poisson's ratio ν_m weakened by ellipsoidal voids.

The central point of the inverse problem construction correlates with the hypothesis that whole information on the microstructure of the material is encompassed in the anisotropy of its mechanical properties. In the case of inverse problem applied to the cancellous bone analysis and represented in Fig. 4b, it is assumed that the apparent global orthotropic properties of a bone sample are known from experimental measurements for instance. The goal is to find the elastic properties of the bone tissue constituting trabeculae and, as auxiliary results, the best representation of the bone sample microarchitecture and the local stress and strain fields. As mentioned above, in this work it is supposed that the bone tissue is isotropic and described by its Young's modulus and Poisson's ratio, E_m and ν_m, respectively. However, the proposed method can be applied to more complex (anisotropic) constitutive behaviors.

2.3. Inverse problem

IS scheme can be projected as a certain function Γ^{IS}, whose arguments are the parameters describing the VE microstructure (μP) and mechanical properties of the matrix (E_m, ν_m).

$$\boldsymbol{C}^{\mathrm{IS}} = \Gamma^{\mathrm{IS}}(\mu P, E_m, \nu_m). \tag{2.5}$$

As a result, the approximations of elastic moduli E_1, E_2, E_3, G_{23}, G_{31}, G_{21}, ν_{23}, ν_{13} and ν_{12} can be extracted from the stiffness tensor C^{IS} provided by the IS-model. The main difficulty of this optimization problem lies in the fact that the computation time to determine the best solution of the function Γ^{IS} rises exponentially with increasing number of microstructural parameters μP. Moreover, since the apparent orthotropic elastic properties of the cancellous bone are defined by nine moduli, this Optimization Algorithm (OA) belongs to the so-called multi-criterial task.

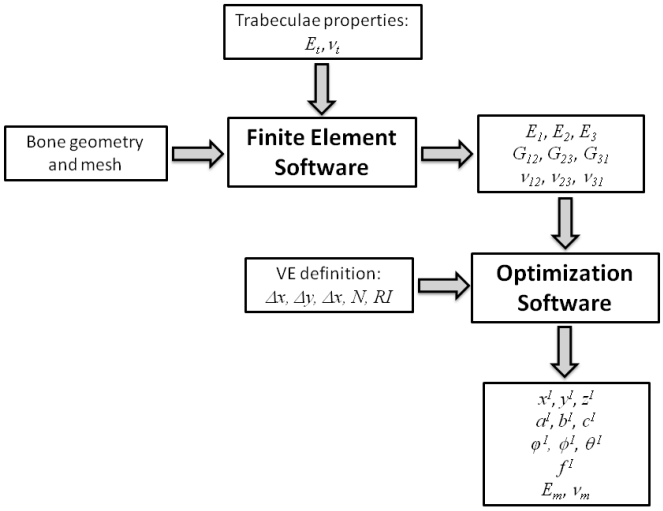

FIG. 5. Algorithmic scheme describing the optimization process of the model parameters.

The validation of the method proposed in this paper is done by comparing the results provided by the optimization algorithm coupled with the IS and the output data of numerical or FE homogenizations. The applied procedure is sketched in Fig. 5.

To carry out the optimization process, the value of the average error of fitting parameters ($\mathrm{err}_{\mathrm{fit}}$) is chosen as a criterion. The whole problem consists in finding the microstructural parameters of the model for which the relative error of fitting parameters is the least.

In the present work, this error value is defined by the average of individual errors of apparent elastic properties and bone porosity:

$$\text{err}_{\text{fit}} = \frac{1}{N_p} \sum_{i=1}^{N_p} \frac{|P_i - p_i|}{P_i} \tag{2.6}$$

where P_i is the reference value of the ith parameter, p_i represents the value of the ith parameter obtained with the IS model, N_p corresponds to the number of parameters to be evaluated.

Because of the high number of microstructural parameters ($N_p = 42$ in the case of $N = 4$), the uniqueness of the solution is surely questionable. A direct sampling of such a large space of alternative solutions with the use of traditional methods is not effective. For this purpose, the optimization algorithm is well adapted. Because of the big number of optimized parameters a genetic algorithm [35] was used to solve the problem.

2.4. Genetic algorithm implementation

The genetic algorithm population is peopled by individuals representing possible solutions of the inverse problem. Each individual consists of the matrix and N ellipsoidal inclusions (see Fig. 6a). The matrix is represented by the size of representative VE (3 independent values for 3 dimensions) and its mechanical properties described by two values: Young's modulus and Poisson's ratio (see

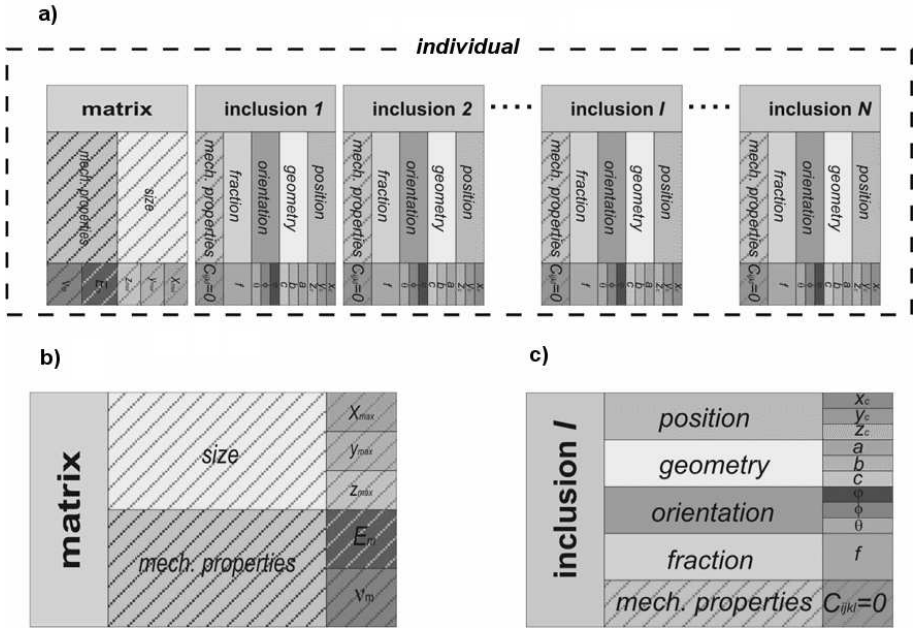

FIG. 6. Definition of individuals.

Fig. 6b). Each inclusion (see Fig. 6c) is represented by position of its centre (3 values), lengths of ellipsoid axes (3 values), orientation of main axes (3 values of Euler angles) and the its volume fraction (one value). The mechanical properties of the inclusions are set to zero because they represent the void although the algorithm may be extended to the case with not void reinforcements. For a single solution an individual is described by $N_p = 10N + 2$ values. All values are represented inside the individual as floating-point numbers.

The initial population is generated by random choice of all individual parameters. Each parameter has a given range of possible values. However, this constrain is not sufficient concerning size and position of inclusions. From the theoretical viewpoint (calculation of $\boldsymbol{T}^{\mathrm{IJ}}$) all inclusions in the solution have to be separated. Sometimes the random procedure can generate a pattern of inclusions with two or more of them partially overlapped. To prevent this occurrence, special iterative procedure was developed. For the intersecting inclusions some parameters (position, shape or/and orientation) are modified in random manner as long as inclusions remain overlapped.

The fitness function used in the algorithm is described by Eq. (2.6), where p_i are all unknown parameters inside an individual. The classical ranking selector was used. The crossover process is performed by an uniform method. It means that each parameter of two individuals may be exchanged with the given probability. Two types of mutation operators are used: the micro and macro mutation. The micro-mutation was introduced in order to prevent early convergence in the case of small populations through random increasing the diversity of solutions. The parameters of an individual obtained in the crossover are subjected to the micro-mutation, which involves a small change of their values. In contrary to the micro-mutation, the macro-mutation involves random changes of the parameter in the whole range which the specified parameter can take. Moreover, this mutation of the parameters does not always occur, but only with the precisely determined probability.

After crossover and/or mutation the arrangement of the inclusion can be incorrect (some inclusions may be overlapped). In the case again the correction procedure is applied but now the parameters of the inclusions are not changed in the completely random way, but rather by small corrections of fault parameters.

3. Results and discussion

3.1. Application of the inverse method for determining the elastic constants of trabeculae

The statistical analysis was used to determine the elastic properties of trabeculae and estimate the quality of the obtained results. Global apparent properties

of the bone samples were supposed to be orthotropic following considerations of COWIN [36]. For the testing purposes, they were determined by FE simulations. The following elastic isotropic properties were attributed to the finite elements representing trabeculae: $E_t = 10\,000$ MPa and $\nu_t = 0.3$. They correspond to the average experimental data found in literature [2–5, 37–42]. Table 1 summarizes their values obtained for four samples treated. It appears from this table that the porosity of the samples was fairly similar and relatively high (about 75%). It was admitted that the samples' edges coincided with the axes of the bone orthotropic frame noted (1, 2 and 3). Their association with the longitudinal, transversal and radial directions of the bone orthotropic system is not the same for all samples. Two first specimens are nearly transversal isotropic whereas the samples III and IV seem to by fully orthotropic.

Table 1. Apparent properties of four trabecular bone samples (I to IV) computed by FE homogenization. The elastic moduli are expressed in [MPa].

	I	II	III	IV
E_1	1040	949.3	286.1	1141
E_2	380.9	246.1	1064.4	194.1
E_3	374.3	337.2	402.6	472.3
G_{23}	211.6	232.0	310.8	92.4
G_{31}	347.5	308.7	205.6	306.1
G_{12}	258.1	243.2	311.0	210.2
ν_{23}	0.248	0.255	0.241	0.161
ν_{13}	0.439	0.326	0.287	0.375
ν_{12}	0.290	0.429	0.110	0.430
Porosity	0.74	0.77	0.76	0.75

The inverse method was successfully applied to all the samples. The optimization procedure was executed exploiting a PC with four ellipsoidal inclusions ($N = 4$) simulating bone porosity. Though, in this paper only the outcomes concerning the first sample are presented and discussed. Young's and shear moduli and Poisson's ratios were deduced from tensors of elastic constants of the VE and were treated as the input data for the optimization procedure. Figure 7 illustrates the comparison of the side views of the real sample I (top line) and its microstructural representation (bottom line) corresponding to the best individual characterized by the fitness error $\mathrm{err}_{\mathrm{fit}} = 2.1\%$. NB: The size of ellipsoids (bottom line) was intentionally diminished to make images clearer and more transparent. Also, notice that, for top line, bone is coloured in grey and, for bottom one, voids are printed in grey.

A basic cell of the structure with inclusions was copied three times in each direction in order to obtain a periodic structure, which was consistent with the

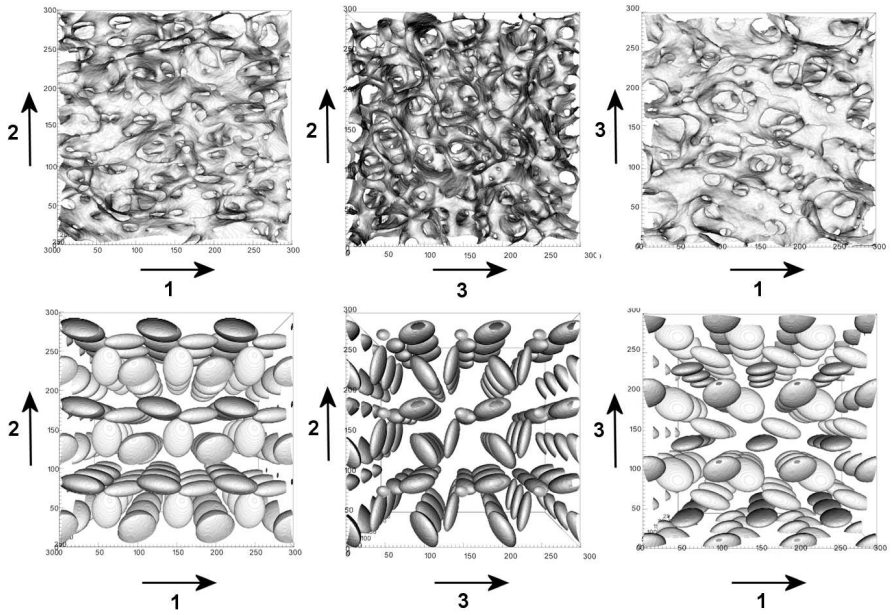

Fig. 7. Comparison of the real trabecular bone (top line) and its representation (bottom line) obtained by the optimization. Bone matter and inclusions are colored in grey, respectively in top and bottom lines.

VE used in FEM calculations. For the definition of the microstructure of cells, readers are referred to Table 2. Instead of the three Euler's angles characterising the inclusions' orientation, three unite vectors $\vec{u}$, $\vec{v}$ and $\vec{w}$ defining the system of principal axes of ellipsoids are gathered in this table. Also, to better understand the shape of inclusions, the ratios of semi axes a/c and b/c are presented.

In spite of the relatively poor representation of the bone by four inclusions, important analogies with the real structure are easily noticeable. For instance, it appears that in plane (1–2), the ellipsoids are arranged in two rows parallel to direction 1. The first row consists of strongly prolate and oblate inclusions of family 1 and 2, respectively. They are represented in dark-grey in Fig. 7. The major axis of the prolate ellipsoid is nearly parallel to the direction 1 whereas the minor axis of the oblate inclusion is almost parallel to the direction 3. Their volume fractions are respectively equal to $f^1 = 0.113$ and $f^2 = 0.165$. Inclusions 3 and 4, plotted in light grey, build the second row. The inclusion 3 is quasi spherical with the biggest volume fraction of $f^3 = 0.278$. The last inclusion has the general ellipsoidal shape, with three different semi axes, and the volume fraction of $f^4 = 0.185$. Its major axis v is mainly oriented in direction 2. In the plane (2–3) no privileged arrangement of inclusions could be identified (at least visually). The view (1–3) confirms the conclusions drawn from the projection (1–2).

Table 2. Micro-architectural parameters of the periodic cell obtained for the best individual.

	Inclusion			
Parameter	1	2	3	4
x^{I}	4.460	5.742	1.151	7.446
y^{I}	3.678	9.767	0.768	3.323
z^{I}	7.980	2.450	4.748	9.956
f^{I}	0.113	0.165	0.278	0.185
a/c	0.793	2.704	1.062	0.527
b/c	0.365	1.965	0.798	1.532
u_1	0.291	−0.959	0.303	0.662
u_2	0.446	−0.284	0.895	0.102
u_3	−0.846	0.005	−0.328	−0.743
v_1	0.304	−0.284	0.898	0.326
v_2	−0.882	0.958	−0.153	0.853
v_3	−0.361	−0.035	0.412	0.408
w_1	−0.907	0.005	0.318	0.675
w_2	−0.152	−0.035	−0.419	−0.512
w_3	−0.392	−0.999	−0.850	0.531

Obviously, these observations are consistent with the apparent elastic properties of the VE given in Table 1.

As indicated by the algorithm of Fig. 5, the matrix properties (E_m, ν_m) belonged to the output of the procedure and were therefore compared with the initial data introduced into the FEM simulation. This comparison was the basis of statistical analysis of the method performances. Genetic algorithms belong to a group of non-deterministic methods, which means that for the same input parameters, different results can be obtained in successive solutions or runs. The best 218 solutions with $\mathrm{err}_{\mathrm{fit}}$ smaller than 5% were selected from all the collected results. The statistical treatment of obtained values of the elastic properties of the matrix is summarized in Fig. 8.

The graphs of this figure testify that the most often (82%) obtained values of Young's modulus of the matrix were in the range from 900 to 1100 MPa. Also, for the majority of solutions, the relative fitness error of Young's modulus of the matrix was below 10%. The important observation is that the better fitness of the effective mechanical properties gives the better fitness of Young's modulus of the matrix (Fig. 8b). For the best solutions, the average error of the fitness of this modulus was about 5%. In the case of Poisson's ratio, in most situations the algorithm overestimated its value. The most often obtained value was about 0.35. The average fitness error of this ratio was ca. 20% and was

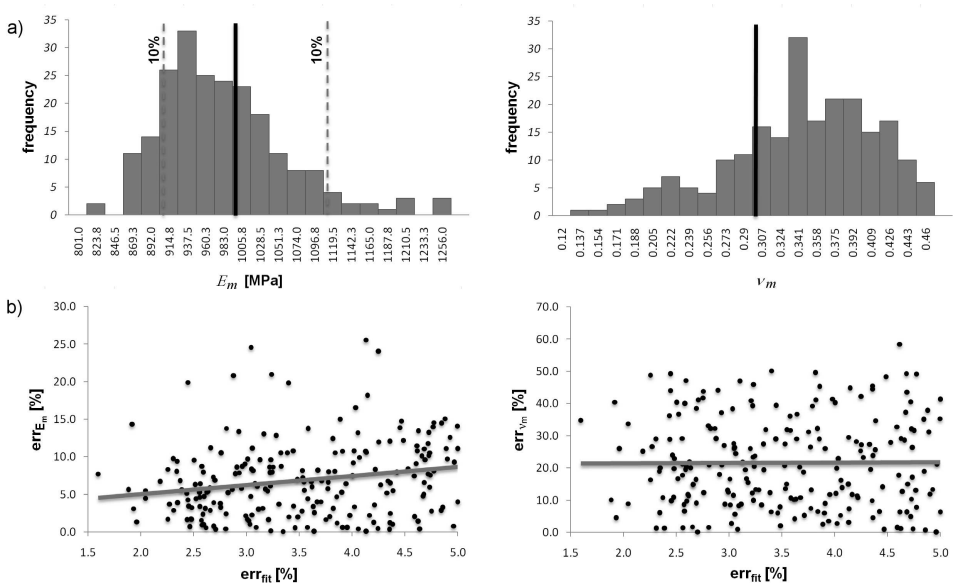

Fig. 8. Summary of the obtained values of Young's modulus and Poisson's ratio of the matrix: a) statistical distributions of the values of the parameters, b) relative error versus fitness function.

independent from the value of the $\mathrm{err}_{\mathrm{fit}}$. This can be explained by the fact that an individual trabecula is mostly isolated from the neighbouring struts by pores so its transversal deformation is only partly transferred to them. In the sequel, the sensibility of the proposed approach is analysed. First the influence of the elastic properties of the trabeculae (matrix) on the fitness function is examined.

3.2. Influence of the mechanical properties of the matrix on the apparent mechanical properties of porous media

Coming back to Eq. (2.5), the value of the function Γ^{IS} depends on the mechanical properties of the matrix. In order to check the influence of the elastic properties of the trabeculae (matrix), two series of simulations were carried out with the incremental scheme and FE homogenization for the frozen microstructure of VE illustrated in Fig. 7. For the first series, Poisson's ratio was kept constant ($\nu_m = \nu_t = 0.3$) and Young's modulus was changed in the large range determined for wet and dry trabecular bones [10] :

$$1 \leq E_m = E_t \leq 16 \text{ GPa}. \tag{3.1}$$

The second series was done for $E_m = E_t = 1$ GPa and Poisson's ratio covering the interval:

$$0.15 \leq \nu_m = \nu_t = \leq 0.45. \tag{3.2}$$

FEM computations were done only for seven combinations of ν_m and E_m values due to a considerable calculation time. As expected, the obtained values of the apparent Young's and shear moduli were very nearly proportional to Young's modulus of the trabeculae (matrix). It can thus be deduced that the ratio of apparent elastic moduli is practically not affected by the modification of E_m. Consequently, apparent Poisson's ratios also do not depend on the value of Young's modulus E_m. Consequently, one can conclude that the relative fitness error of these parameters is constant and does not depend on the value of Young's modulus of the matrix. Differences between FEM and IS predictions are only due to the quality of the fitness of the microstructure. In the case of sample I, the biggest discrepancy concerns G_{23} shear modulus.

The plots in Fig. 9 present the values of the apparent mechanical properties determined with the IS model and by FEM homogenization.

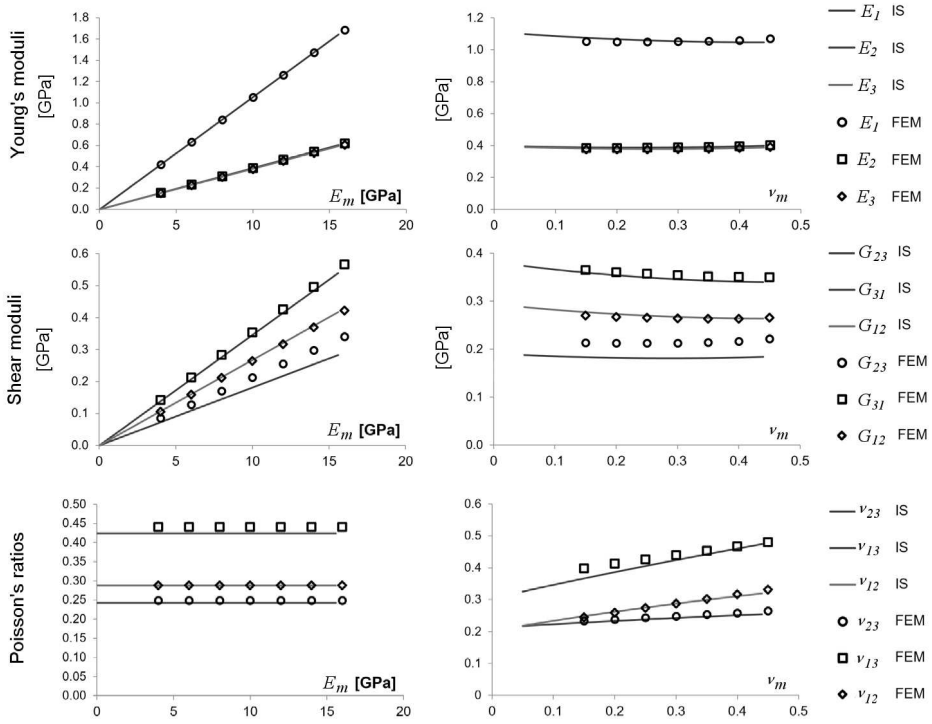

FIG. 9. Comparison of the global elastic moduli and Poisson's ratios predicted by IS and FEM as a function of elastic properties of the matrix.

The analysis of the influence of Poisson's ratio of the trabeculae (matrix) on the apparent elastic properties determined by IS and FEM reveals small changes of global Young's and shear moduli. This can be once again explained by the

fact that an individual trabecula is surrounded by pores and globally isolated from the neighbouring struts. Consequently, its transversal deformation is not transferred to the adjacent trabeculae.

It also appears from Fig. 9 that ν_m has more influence on the apparent Poisson's ratios of the tested microstructure. However, the variability of some of these ratios exceeded 50%. Therefore, no real tendency can be obtained from this last series of tests. More deepened discussion of these results can be found in reference [43]. As a rule, high consistency between IS and FEM was obtained except once again for shear modulus G_{23}. The dependence of ν_{13} Poisson's ratio on ν_m was also less precisely described by the IS model.

Finally, this analysis revealed that the degree of anisotropy of the sample is almost independent of Young's modulus and Poisson's ratio of the matrix (trabeculae). The value of Young's modulus of the trabeculae (matrix) controls the level of the apparent properties of the sample and its Poisson's ratio has no significant influence on the apparent properties of the VE.

3.3. Influence of porosity

In this section, the influence of the sample porosity on the quality of predicted values of the trabecular bone apparent properties was examined. To this end, the elastic properties of the matrix were fixed to $E_m = 10$ GPa and $\nu_m = 0.3$, both for the IS and FE models. All microstructural parameters, except the porosity, were also frozen. To change the porosity in IS model, a proportional decreasing or increasing of size of all ellipsoids was performed to obtain the desired value of the total volume fraction of inclusions. Location and orientation of the inclusions remained the same.

In the case of FEM homogenization, in order to obtain different porosities for the given microstructure, the graphical filters of erosion and dilatation were used to modify the two-dimensional scans. The dilatation filter "thickens" the walls, and the erosion filter causes their "thinning" (Fig. 10). Using a particular

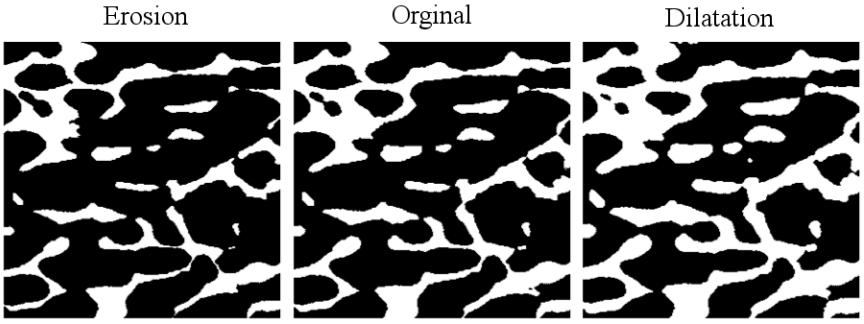

Fig. 10. The effect of erosion and dilatation on the original image.

filter repeatedly, various porosities could be obtained. In the case of using the erosion filter, the occurrence of "lost struts" (i.e. struts with no contact with the other ones) was checked. If such elements were found, they were removed from the concerned images.

Five different 3D objects were next built from the so-prepared series of scans. After meshing, the mechanical apparent properties were calculated using FEM homogenization. In order to verify how correctly the IS model can determine the elastic properties for a given microstructure with varying porosity, the IS results were once again compared with FEM predictions. They are illustrated in Fig. 11.

It can be deduced from this figure that, for all tested porosities, very good agreement was reached for all Young's and shear moduli. Poisson's ratios were fitted relatively well but not as well as Young's and shear moduli. Ultimately,

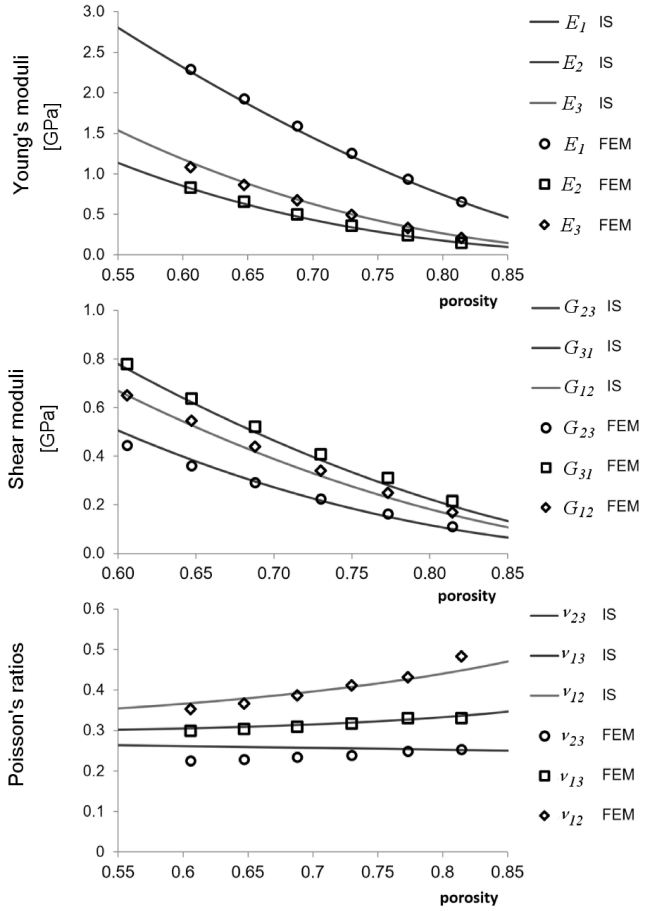

FIG. 11. Values of the effective elastic properties in function of porosity for the IS and FEM models.

one can conclude that, for the tested microstructures, the results obtained from the IS model are in good accordance with FEM predictions.

3.4. Influence of microstructure fitting

This paragraph presents the statistical analysis concerning the influence of microstructure fitting on the apparent properties of the sample. Basing on the comments formulated in the previous paragraphs, this analysis was performed using the partial inverse approach illustrated in Fig. 12. The elastic properties of the matrix were supposed to be known and identical to those of the trabeculae used in FE simulations.

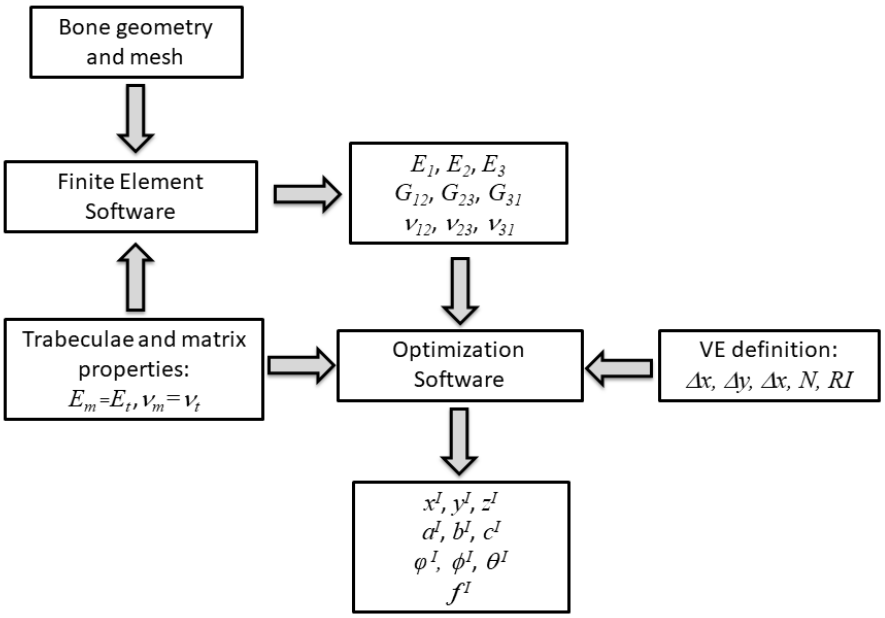

FIG. 12. Simplified algorithm of the bone microarchitecture fitting.

The test was done to check if one could obtain a microstructure for which the function Γ^{IS} gives a reasonable value of average error $\mathrm{err}_{\mathrm{fit}}$ with imposed elastic properties of the matrix. The test was conducted for the following matrix properties:

$$E_m = E_t = 1 \text{ GPa}, \qquad \nu_m = \nu_t = 0.3, \tag{3.3}$$

178 best solutions with $\mathrm{err}_{\mathrm{fit}}$ smaller than 5% were selected from all the collected results. They form a reduced set of solutions fulfilling the specified convergence criterion, simple to study. Because $\mathrm{err}_{\mathrm{fit}}$ was calculated from the mean value of errors of porosity and nine apparent elastic constants, it is not possible to

Table 3. Listing of the statistically best solutions for which the error of fitting mechanical parameters was smaller than 5%. Data from reduced set of 178 solutions. The value of $\mathrm{err}_{\mathrm{fit}}$ for the best individual is 2.1%.

FEM		Optimization Algorithm				
Parameters		Best individual		Mean		Deviation
		value	err [%]	value	err [%]	
Porosity	0.74	0.75	1.9	0.76	3.2	0.0083
E_1 [MPa]	104.0	104.0	0.0	104.8	0.8	2.1
E_2 [MPa]	38.0	38.5	1.3	38.1	0.3	0.57
E_3 [MPa]	37.4	39.5	5.5	38.8	3.8	1.4
G_{23} [MPa]	21.2	19.6	7.2	18.1	14.1	0.92
G_{31} [MPa]	34.8	34.3	1.3	32.7	5.9	1.5
G_{21} [MPa]	25.8	25.6	0.7	26.1	1.3	0.47
ν_{23}	0.238	0.244	1.1	0.247	0.1	0.0040
ν_{13}	0.439	0.439	0.0	0.426	2.9	0.0150
ν_{12}	0.290	0.290	0.1	0.287	0.8	0.0059

conclude from its value alone if the error is distributed uniformly on all the parameters or if it is mainly concentrated on several among them. Table 3 presents the best individual from the set studied defined by the 10 parameters involved in $\mathrm{err}_{\mathrm{fit}}$ calculations. Also, the average value and standard deviation as well as the FEM results are collected in this table for every parameter.

Important conclusions can be drawn from Table 3. The error was not distributed uniformly over all parameters. Indeed, for the shear modulus G_{23} the difference between the average value of the parameter obtained using the model and the value determined with FEM was relatively significant (about 14%). The obtained values of G_{23} were underestimated and even the maximum value of this module (not given here) was smaller than the value from FEM. The shear modulus G_{31} was another relatively poorly fitted parameter but, in comparison with the parameter G_{23}, the average relative error was 2.5 times smaller. Among Young's moduli, E_3 was characterized by a poorer precision. An error of 3.8% was found by comparing its average value with the FE prediction. The level of fitness for Poisson's ratios was comparable with the fitness of Young's moduli. The values of porosity were slightly overestimated by the model (of about 3%). It was mainly due to relatively small number of steps (20) used in Incremental Scheme.

The same analysis was performed on four different samples. For all of them, similar values of parameters were found. The value of $\mathrm{err}_{\mathrm{fit}}$ was, in each case, about few percents, but the distribution of the error depended on the sample. It was found that the shear moduli were always the most poorly fitted.

Presented results led to main conclusion that, if the mechanical properties of the matrix are known, one can find a microstructure for which the apparent elastic properties obtained from the IS are consistent with FEM predictions. The results also showed that, under the hypothesis of isotropic elastic properties of the matrix, the determination of the microstructure of the bone could be dissociated from the fitting of the matrix properties. However, in the case of experimentally determined average properties of bone volume, the bone tissue properties are unknown. Consequently, the full inverse method must be applied to determine simultaneously the elastic properties of the trabeculae and the micromechanical representation of the bone microarchitecture.

3.5. General comments

In the modelling approach presented in this work, it was assumed that the mechanical properties of a trabecular tissue were isotropic. Concerning the IS scheme, the anisotropy of the trabeculae can be easily taken into account. However, problems occur during FEM simulation because one has to change the orientation of anisotropy frame locally. Further works need to be undertaken in this area. The developed approach treating the bone as a composite material and determining its effective mechanical properties through the incremental scheme based homogenization method gives accurate results, in the case of trabecular bone modeling compared to the FEM predictions. The main advantage of the IS is its calculation time, which is several orders of magnitude shorter than FEM. In the case of the inverse method, the determination of the microarchitectural parameters by the IS is time consuming but it is performed only once for a given structure. Some observations made during the study seem to suggest that it might be possible to find correlations between the microstructure of the elementary volume and the real bone microarchitecture. If so, the microstructure determination process would be much faster. In that case, the proposed method could be applied also for other porous materials. For the best-fitted microstructures, the value of the error $\mathrm{err}_{\mathrm{fit}}$ was about 2%, but even in this case the distribution of the error between all elastic constants was not homogenous. As a consequence, one has to wonder if such a criterion of the choice of optimal solution is the best one. Another possibility would be to try to find microstructures, by minimizing the biggest error of the fitted parameter.

4. Conclusions

First of all, the ability of the incremental scale transition model, combined with an optimization algorithm, to determine the apparent properties of the cancellous bone has been demonstrated in the present paper. It was observed

that the anisotropy of the bone sample is almost independent from the properties of the matrix and is mainly due to the bone microarchitecture. This conclusion is of major interest because it guarantees that an ellipsoidal representation found for a given bone structure with supposed matrix mechanical properties will be valid also for other values of matrix properties. From practical point of view, this statement gives possibilities to divide trabecular bone tissue modeling into two steps:

1. find the best ellipsoidal representation of its microarchitecture (even if Young's moduli and other mechanical parameters are not strictly precise);

2. determine the best mechanical properties of the matrix with the fixed microstructural representation.

Such an approach can significantly accelerate the optimization process.

On the other hand, the use of the incremental scheme combined with an optimization algorithm for determining the isotropic elastic properties of the cancellous bone trabeculae gave satisfactory results. The best results provided an average error of about 5% between obtained Young's modulus of the matrix and its reference value. In the case of Poisson's ratio, the error was equal to 20%, but it did not depend on the fitness of the concerned microstructure. Moreover, although the quality of the fitness of the matrix Poisson's ratio is low, it should be noted that its influence on the effective or apparent mechanical properties is limited. The developed approach is destined to build reliable FE models of bone organs, taking into consideration the heterogeneity of bone properties on a macroscopic level. The necessity of a fine description of the mechanical property gradient is important e.g. in estimating the risk of fracture or in designing patient specific implants.

Acknowledgements

Three of the authors (KJ, SW and JT) wish to acknowledge the Polish National Science Centre and the Ministry of Science and Higher Education for their financial support under the grant NCN 2017/26/E/ST5/00043.

References

1. R.B. Ashman, S.C. Cowin, W.C. Van Buskirk, J.C Rice, *A continuous wave technique for the measurement of the elastic properties of cortical bone*, Journal of Biomechanics, **17**, 5, 349–361, 1984.

2. P.K. Zysset, X.E. Guo, C.E. Hoffler, K.E Moore, S.A. Goldstein, *Elastic modulus and hardness of cortical and trabecular bone lamellae measured by nanoindentation in the human femur*, Journal of Biomechanics, **32**, 1005–1012, 1999, doi:10.1016/S0021-9290(99)00111-6.

3. J.Y. Rho, R.B. Ashman, C.H. Turner, *Young's modulus of trabecular and cortical bone material: ultrasonic and microtensile measurements*, Journal of Biomechanics, **26**, 111–119, 1993, doi:10.1016/0021-9290(93)90042-D.

4. C.H. Turner, J.Y. Rho, Y. Takano, T.Y. Tsui, G.M. Pharr, *The elastic properties of trabecular and cortical bone tissues are similar: results from two microscopic measurement techniques*, Journal of Biomechanics, **32**, 437- 441, 1999, doi:10.1016/S0021-9290(98)00177-8.

5. S. Lorenzetti, R. Carretta, R. Müller, E. Stüssi, *A new device and method for measuring the elastic modulus of single trabeculae*, Medical Engineering & Physics, **33**, 993–1000, 2011.

6. L.J. Gibson, M.F. Ashby, *The mechanics of 3-dimensional cellular materials*, Proceeding of the Royal Soiety of London, A, **382**, 43–59, 1982.

7. G. Bevill, S.K. Easley, T.M. Keaveny, *Side-artifact errors in yield strength and elastic modulus for human trabecular bone and their dependence on bone volume fraction and anatomic site*, Journal of Biomechanics, **40**, 3381–3388, 2007.

8. D. Van Rietbergen, B. Weinans, R. Huiskes, A. Odgaard, *A new method to determine trabecular bone elastic properties and loading using micromechanical finite-element models*, Journal of Biomechanics, **28**, 69–81, 1995.

9. D. Ulrich, D. Van Rietbergen, H. Weinans, H. Ruegsegger, *Finite element analysis of trabecular bone structure: a comparison of image-based meshing techniques*, Journal of Biomechanics, **31**, 1187–1192, 1998.

10. Ł. Cyganik, M. Binkowski, G. Kokot, T. Rusin, P. Popik, F. Bolechała, R. Nowak, Z. Wróbel, A. John, *Prediction of Young's modulus of trabeculae in microscale using macro-scale's relationships between bone density and mechanical properties*, Journal of the Mechanical Behavior of Biomedical Materials, **36**, 120–134, 2014.

11. S. Ilic, K. Hackl, K.R. Gilbert, *Application of the multiscale FEM to the modeling of cancellous bone*, Biomechanics and Modeling in Mechanobiology, **9**, 87–102, 2010.

12. P. Kowalczyk, *Elastic properties of cancellous bone derived from finite element models of parameterized microstructure cells*, Journal of Biomechanics, **36**, 961–972, 2003.

13. M.J. Silva, L.J. Gibson, *Modeling the mechanical behavior of vertebral trabecular bone: effects of age-related changes in microstructure*, Bone, **21**, 191–199, 1997.

14. W. Voigt, *Ueber die Beziehung zwischen den beiden Elasticitätsconstanten isotroper Körper*, Annals of Physics, **38**, 185–192, 1889.

15. A. Reuss, *Berechnung der Fließgrenzevon Mischkristallen auf Grund der Plastizittatsbedingung fur Einskristalle*, Journal of Applied Mathematics and Mechanics, **9**, 49–58, 1929.

16. R. Hill, *A self-consistent mechanics of composite materials*, Journal of the Mechanics of Solids, **13**, 213–222, 1965.

17. P.H. Dederichs, R. Zeller, *Variational treatment of the elastic constants of disordered materials*, Journal of Solid State Physics, **259**, 103–113, 1973.

18. J.R. Willis, *Variational and related methods for the overall properties of composites*, Advances in Applied Mechanics, **21**, 1–78, 1981.

19. L.J. WALPOLE, *Elastic behaviour of composite materials: theoretical foundations*, Advances in Applied Mechanics, 169–242, 1981.

20. O. FASSI-FEHRI, A. HIHI, M. BERVEILLER, *Multiple site self consistent scheme*, International Journal of Engineering Science, **27**, 495–502, 1985.

21. P. LIPINSKI, *Modélisation du comportement des métaux, en transformations élastoplastiques finies, à partir des méthodes de transition d'échelles*, Habilitation Thesis, Université de Metz, Metz, 1993.

22. T. MORI, T. TANAKA, *Average stress in matrix and average elastic energy of materials with misfitting inclusions*, Acta Metallurgica, **21**, 571–574, 1973.

23. E. KRÖNER, H. KOCH, *Effective properties of disordered materials*, Symposium on Micromechanics Archives, **1**, 183–238, 1976.

24. E. KRÖNER, *Bounds for effective elastic moduli of disordered materials*, Journal of the Mechanics of Solids, **25,** 137–155, 1977.

25. A. BROOHM, P. ZATTARIN, P. LIPINSKI, *Prediction of mechanical behavior of inhomogeneous and anisotropic materials using an incremental scheme*, *Archives of Mechanics*, **6**, 949–967, 2000.

26. D.A.G. BRUGGEMAN, *Berechnung verschiedener physikalischer Konstante von heterogene Substanzen*, Annuals of Physics, **416**, 636–664, 1935.

27. P. VIÉVILLE, P. LIPINSKI, *Application du schéma autocohérent par étapes à la modélisation des propriétés viscoélastiques des composites*, [in:] J.P. Favre, A. Vautrin [eds.], AMAC, JNC9 Saint-Etienne, France, **9**, 545–554, 1994.

28. L.A. FELDKAMP, L.C. DAVIS, J.W. KRESS, *Practical cone-beam algorithm*, Journal of the Optical Society of America, **A6**, 612–619, 1984.

29. *Reference Manual VGStudio Max Release 2.0*, Volume Graphics GmbH Editor, 2013, http://www.volumegraphics.com/en/products/vgstudio-max/8.10.

30. M. DOUBE, M.M. KŁOSOWSKI, I. ARGANDA-CARRERAS, F. CORDELIÉRES, R.P. DOUGHERTY, J. JACKSON, B. SCHMID, J.R. HUTCHINSON, S.J. SHEFELBINE, *BoneJ: free and extensible bone image analysis in ImageJ*, Bone, **47**, 1076–1079, 2010.

31. N. OTSU, *A threshold selection method from fray-level histograms*, IEEE Travsactions on Systems, Man and Cybernetics, **SMC9 l**, 62–66, 1979.

32. K. JANC, J. KAMINSKI, J. TARASIUK, A.S. BONNET, P. LIPINSKI, *Homogenization of trabecular bone microstructure based on finite element method and micro computed tomography*, 11th World Congress on Computational Mechanics (WCCM XI), Barcelona, Spain 1012–1017, 2014.

33. W. AZOTI, Y. KOUTSAWA, N. BONFOH, P. LIPINSKI, S. BELOUETAR, *On the capability of micromechanics models to capture the auxetic behavior of fibers/particles reinforced composite materials*, Composites Structures, **94**, 156–165, 2011.

34. P. VIÉVILLE, A.S. BONNET, P. LIPINSKI, *Modeling effective properties of composite materials using the inclusion concept. General considerations*, Archives of Mechanics, **58**, 207–239, 2001.

35. J.H. HOLLAND, *Adaptation in Natural and Artificial System*, The University of Michigan, Press MIT Press Cambridge, MA, U.S.A., 1992.

36. S.C. Cowin, M.M. Mehrabadi, *Identification of the elastic symmetry of bone and other materials*, Journal of Biomechanics, **22**, 503–515, 1989.

37. P. Zioupos, R.B. Cook, J.R. Hutchinson, *Some basic relationships between density values in cancellous and cortical bone*, Journal of Biomechanics, **41**, 1961–1968, 2008.

38. B. Helgason, E. Perilli, E. Schileo, F. Taddei, S. Brynjolfsson, M. Viceconti, *Mathematical relationships between bone density and mechanical properties, A literature review*, Clinical Biomechanics, **23**, 135–146, 2008.

39. E. Cory, A. Nazarian, V. Entezari, V. Vartanians, R. Muller, B.D. Snyder, *Compressive axial mechanical properties of rat bone as functions of bone volume fraction, apparent density and micro-ct based mineral density*, Journal of Biomechanics, **43**, 953–960, 2010.

40. H. Follet, S. Viguet-Carrin, B. Burt-Pichat, B. Dépalle, Y. Bala, E. Gineyts, F. Munoz, M. Arlot, G. Boivin, R.D. Chapurlat, P.D. Delmas, M.L. Bouxsein, *Effects of preexisting microdamage, collagen cross-links, degree of mineralization, age, and architecture on compressive mechanical properties of elderly human vertebral trabecular bone*, Journal of Orthopaedic Research, **29**, 481–488, 2011, doi:10.1002/jor.21275.

41. E. Hamed, I. Jasiuk, A. Yoo, Y.H. Lee, T. Liszka, *Multi-scale modelling of elastic moduli of trabecular bone*, Journal of the Royal Society Interface, **9**, 1654–1673, 2012, doi:10.1098/rsif.2011.0814.

42. S.N. Musy, G. Maquer, J. Panyasantisuk, J. Wandel, P.K. Zysset, *Not only stiffness, but also yield strength of the trabecular structure determined by non-linear* μFE *is best predicted by bone volume fraction and fabric tensor*, Journal of the Mechanical Behavior of Biomedical Materials, **65**, 808–813, 2017.

43. K. Janc, *Micromechanical modeling of bone elastic properties based on computed tomography*, Doctoral Thesis, AGH – University of Science and Technology, Poland, Lorraine University, France, 2013.

Received January 22, 2020; revised version August 25, 2020.
Published online October 16, 2020.